A new method to detect anisotropy and local variations in paper

Kenneth Olofsson and Nils-Erik Molin

Research student and professor, Division of Experimental Mechanics, Lulea University of Technology, S-95187 Lulea, Sweden

Anders Kyosti

Research engineer, SCA Nordliner AB, S-94187 Pitea, Sweden

ABSTRACT *The mechanical properties of paper were studied using holographic interferometry. Bending wave propagation in paper was generated by the impact of a small pendulum. Holograms were produced at various times elapsed after impact with the use of a double-pulsed ruby laser. Results show that this method can be used to detect anisotropy, to determine principle directions (machine and cross-machine), and to examine local variations in paper.*

KEYWORDS
Analysis
Paper properties
Tensile strength
Testing

Measures of strength and stiffness in different directions of the paper are critical quality indicators for paper manufacturers. The industry is currently seeking optical and other noncontact, nondestructive, preferably on-line methods for measuring these qualities. Holographic interferometry (*1*), with a double-pulsed ruby laser light source, has proven to be a competitive tool for the study of transient events like the propagation of bending waves in plates and shells (*2-5*). This method may be applied to the study of paper properties because paper behaves as a plate during and shortly after impact. Indeed, holographic interferometry experiments with paper are surprisingly easy to perform.

We studied wave propagation in plates and paper using holographic interferometry. Results are compared here with those obtained through ultrasonic measurements.

Bending wave propagation in plates

Using the arrangement illustrated in **Fig. 1**, bending waves are created by the impact of a small steel sphere of a ballistic pendulum released from an electromagnet. The steel sphere (5 mm in diameter) passes through the light beam of a HeNe-laser aimed at the photodiode. This interruption of the light beam triggers the ruby laser to send its first laser pulse onto the object plate (the paper sheet), producing the first exposure of a double-exposed hologram. Thus, the first exposure occurs before the pendulum hits the plate.

Soon thereafter, the pendulum impacts the plate and creates transient waves. The next laser pulse is deliberately delayed with respect to the first pulse for 1-800 μs. In this manner, a series of holograms can be recorded by repeating the experiment with increasing time delays.

An electric tape at the impact center is part of an electric circuit containing the pendulum. Pulses from this circuit and from the ruby laser are traced by a two-beam memory oscilloscope. The variable T is assigned as the impact time, or the length of time the sphere is in contact with the plate (which is measured to be 80 μs for aluminum plates and 1.5 ms for paper). The variable t is assigned as the time from the start of impact to the second laser pulse. The pulse length of the ruby laser, or the exposure time, is as short as 25 ns, so even propagating bending waves are recorded "frozen" in the hologram.

In the reconstructed image of this double-exposed hologram, the object plate is covered with a set of cosinusoidal fringes. These interference fringes display contours of equal, out-of-plane displacements of the plate.

In **Fig. 2**, examples are shown of double-exposed interferograms of an impacted aluminum plate obtained with the setup in Fig. 1. The interference rings (fringes) in the figure can be viewed as lines connecting points of equal amplitude, like the iso-curves on a contour map showing hills and valleys. Broad rings either indicate a "hill" or a "valley," since the sign of the rings is ambiguous. The sign of a ring has to be determined from the way the experiments are performed (from the experiment we know the direction of the impulse), based on the assumption of a continuous wave pattern. From the broad rings in the impact center (the smooth top of the hill), the ring density increases outwardly, giving the downhill slope. Further out, the rings broaden again, corresponding to a valley or a moat. Thereafter, the ring density increases and decreases again, corresponding to a ridge. This pattern continues until the wave flattens out into zero amplitude. Two consecutive rings have a difference in amplitude of about half the wavelength (that is, 694.3 nm divided by 2). The smallest detectable amplitude in this setup is about 100 nm. High-frequency components with smaller amplitudes may exist but are not recorded. Note that the ring pattern is circular for this isotropic plate. In **Fig. 3**, the transverse displacement of the same impacted aluminum plate at 100 μ is illustrated together with one half of the corresponding interferogram made in the setup in Fig. 1. This is the way an interferogram is interpreted.

During the impact, the pulse is growing in the center and propagating outwards. After the impact time T and until the waves have reached the edge of the plate, the deflection in the center is constant and the wave is moving outwards as if there were no rim, which implies an initial value problem (compare Fig. 2 at 100 μs). Later, waves start to reflect from the edges then interfere with outgoing ones to create a pattern resembling a standing wave, which suggests a boundary value problem (see Fig. 2 at 300 and 600 μs).

To formulate an analytical description comparable with the measurements presented in Figs 2. and 3, we need to solve the Kirchhoff plate equation for an isotropic plate. The Kirchhoff equation is:

$$D\Delta^4 w + \rho \frac{\partial^2 w}{\partial t^2} = p(r,t) \qquad (1)$$

where

D = plate stiffness (defined in Eq. 7)

ρ = area density

Δ^4 = biharmonic operator

r = radial distance from impact center

t = time from the start of impact

$p(r,t)$ = circular symmetrical load per unit area

w = out-of-plane deflection of the plate of uniform thickness.

This equation has been solved analytically by Fallstrom *et al.* (*3, 4*) when the plate is impacted at one point by

1. Experimental arrangement used to record interferograms of propagating transverse waves in plates. The electromagnet in a pendulum arrangement holds the impacting sphere which hits the object plate from behind.

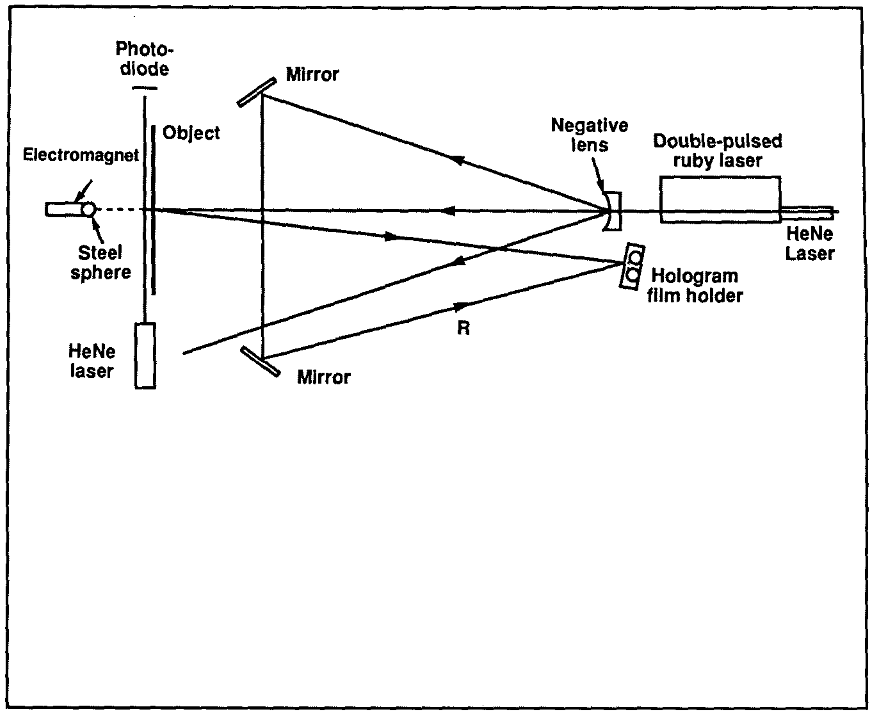

2. Interferograms showing bending wave propagation in an aluminum plate at t = 5, 100, 300, and 600 μs after the start of impact. (Impact time = 80 μs.)

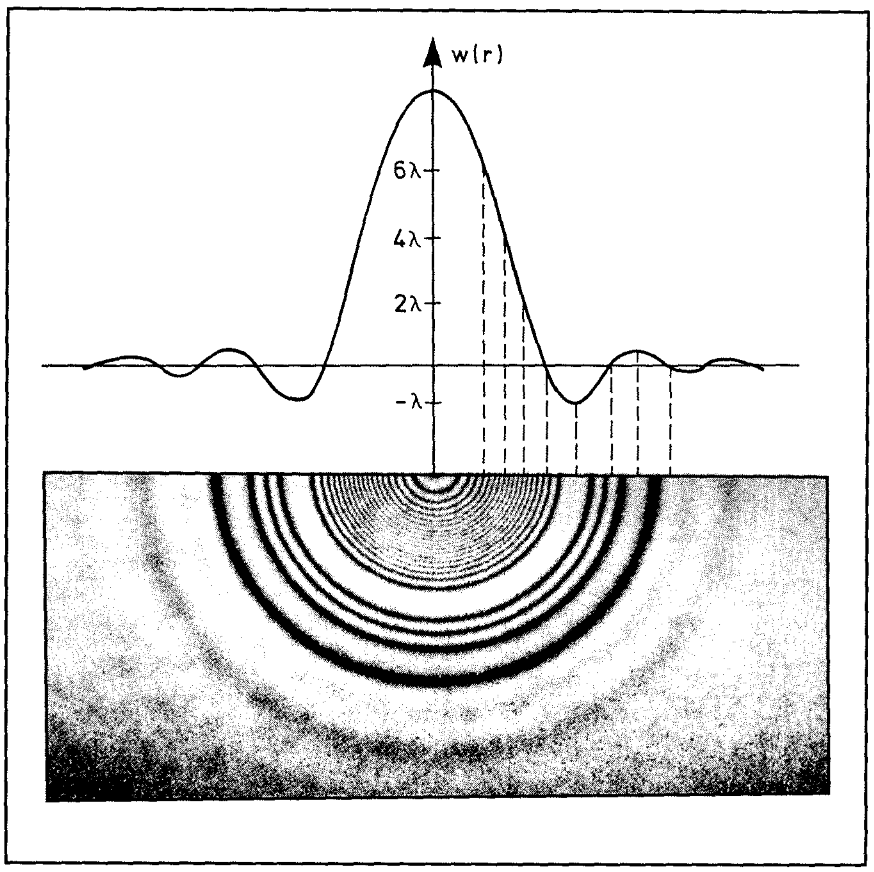

3. Transverse displacement $w(r)$ vs. radial distance from impact center, r, for an aluminum plate at t = 100 μs. (Impact time = 80 μs.)

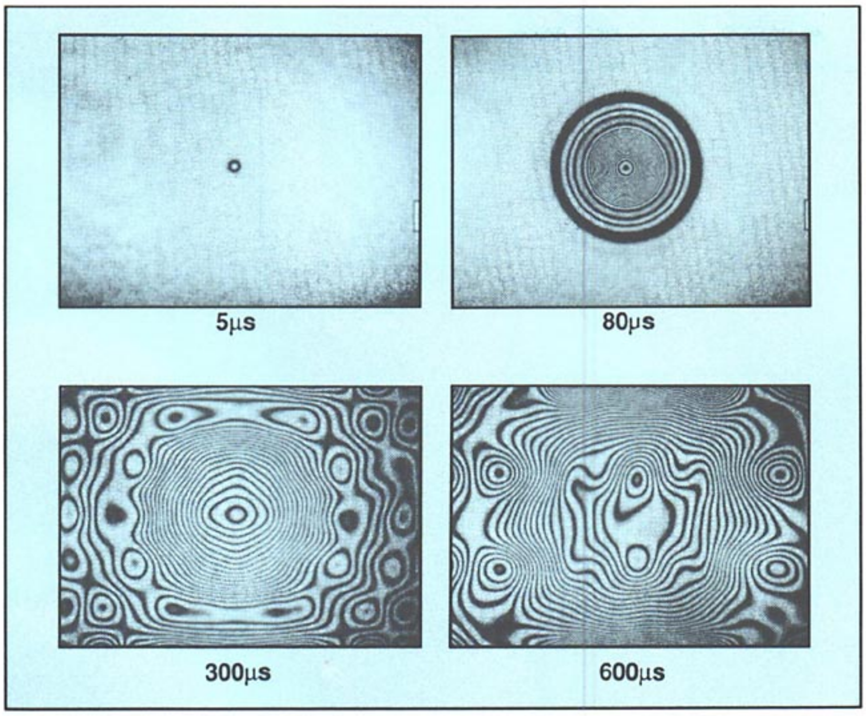

4. Out-of-plane displacement vs. radial distance at 100 μs after the start of impact. The solid line is based on the experimental values from Fig. 3. The dashed line represents a theoretical, point-like contact of infinitesimally short duration where T = O (as for Eq. 2). The dashed and dotted line is also theoretical, where T = 80 μs (as for Eq. 5).

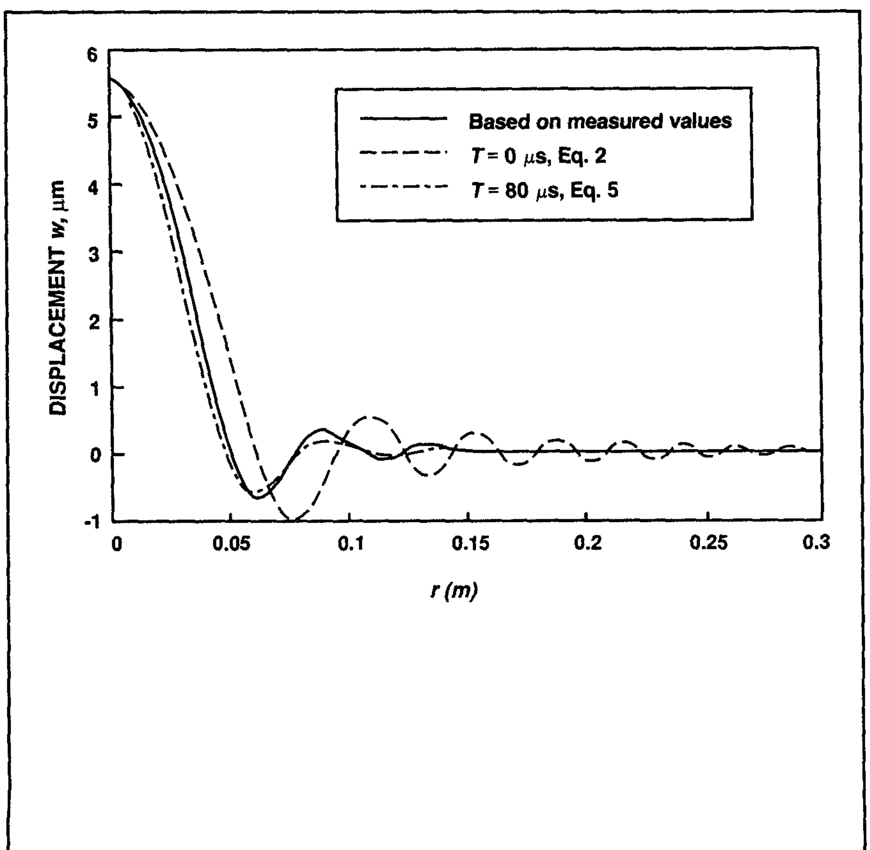

a contact force of infinitesimal duration or by a force of half-sinusoidal duration on the plate. Aprahamian *et al.* (*2*) numerically solved the corresponding Mindlin plate equation to accommodate both rotary inertia and shear deformations, then they compared their mathematical results with empirical data. Fallstrom *et al.* solved the Kirchoff plate equation using Hankel transforms with respect to the radius and using Laplace transforms with respect to time t.

Case A. For a point-like impact of *infinitesimal* duration, the solution of Eq. 1 was found to be

$$w(r,t) = \frac{Ia}{4\pi D}\left[\frac{\pi}{2} - \int_0^{\beta^2/4} \frac{\sin x}{x}\,dx\right] \quad (2)$$

where

I = impulse transferred to the plate during impact by the pendulum.

The variable β is a similarity variable defined as:

$$\beta = r/\,(a\,t)^{1/2} \quad (3)$$

Thus, the out of plane deformation $w(r,t)$ in Eq. 2 is actually a function of β alone, which simplifies the interpretation. The variable a is a plate parameter defined as:

$$a = (D/\rho)^{1/2} \quad (4)$$

The graph of Eq. 2 for a 3-mm-thick aluminum plate at t = 100 μs is shown in **Fig. 4** as a dashed line. In Fig. 4 the variable r (only in this case), can be replaced by the similarity parameter β, as we know the plate parameter a for the aluminum plate and the time t = 100 μs. With this description, we get the displacement w, for all times t and distances r. The pulse is dispersive; it changes shape with time. The broad main peak at constant height in the center is surrounded by ripples with decreasing amplitude and increasing wavelength. High-frequency components travel faster than low-frequency ones.

Case B. For a point-like impact of *half-sinusoidal* duration, where the force varies as half a period of a sinus wave with amplitude A (during the impact time T), the equation for $t > T$ is (*3*):

5. These interferograms show bending wave propagation in two 400-g/m² paper samples. The time elapsed from the start of impact increases for each photograph from left to right. Each of the two series of holograms reveals that the rings expand much like the concentric circles on the surface of a pond when someone throws a rock in the water, but here the wave pattern is not circular.

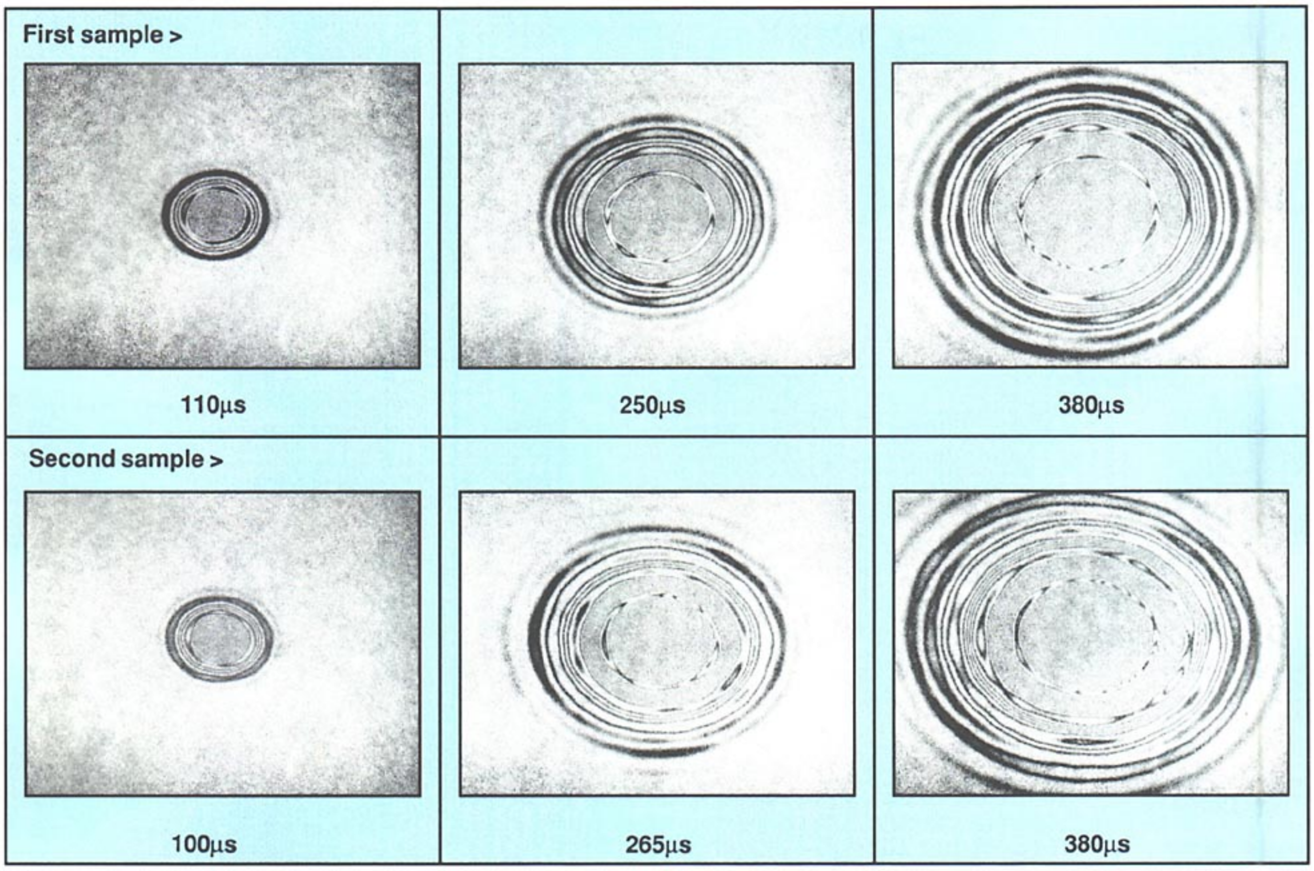

$$w(r,t) = \frac{Aa}{DT}\int_0^{\infty} \frac{J_0(x)}{x} \frac{\sin[ax^2/r^2(t-T/2)]\cos[(ax^2/r^2)(T/2)]}{[(\pi/T)^2-a^2x^4/r^4]}\,dx \quad (5)$$

where

J_0 = the zero-order Bessel function.

When $T \rightarrow 0$, the same result as described by Eq. 2 is obtained. A solution for times $t < T$ is also given by Fallstrom *et al.* (*3*). A graph of Eq. 5, obtained from the same aluminum plate parameters as before with t = 100 μs and T = 80 μs, is represented as a dashed-and-dotted line in Fig. 4. The results are very close to the experimental solid line obtained from the 100-μs picture in Fig. 3, interpreted as in Fig. 2. Anisotropic materials like fiberglass-reinforced plates have also been studied using the same technique, as have defects in wood (*4*, *5*).

I. Comparison of results obtained from the interferograms and ultrasound measurements

		First sample	*Second sample*
Velocity ratios			
From interferograms	$(r_{max}/r_{min})^4$	2.00	2.36
Ultrasonically measured	$(v_{max}/v_{min})^2$	2.40	2.96
Directional angles, °			
From interferograms			
Machine direction	θ_{MD}	8	0
Cross-machine direction	θ_{CD}	6	0
Ultrasonically measured			
Machine direction	ϕ_{MD}	9.1	-1.5
Cross-machine direction	ϕ_{CD}	8.3	-1.5

*Anisotropic directions, measured in degrees relative to the machine direction.

Experiments with paper

Experiments were performed with paper using the same method and setup as illustrated in Fig. 1. The paper used in these experiments was unbleached linerboard with a basis weight of 400 g/m^2 produced on the same fourdrinier paper machine on different occasions.

Two samples were cut to the size of 220 × 260 mm, with the longer side parallel to the machine direction (MD). The main difference between the samples was the principle direction of anisotropy. The paper was attached to a simple rectangular frame of Plexiglas to keep the paper in a fixed position. The dimensions of the frame are 250 × 310 mm on the outside and 170 × 230 mm on the inside. The frame was painted black to avoid light reflections. A small piece of aluminum foil (1 × 1 cm, 0.018 mm thick) was glued at the impact point as part of an electric circuit used to measure the impact time T.

Figure 5 shows three interferograms of each paper. At the top are three pictures taken for three different impacts of the first sample at the elapsed times t after impact start, as given. Impacts were gentle, and no damage to the sample can be observed. At the bottom are pictures of the second sample. The impact time T in both experiments was about 1.5 ms.

The interferograms in Fig. 5 are recorded at times less than the impact time (i.e., $t < T$). The pendulum is still in contact with the paper and is still transferring energy and momentum to it. The central peak is thus growing in amplitude, while the outermost rings are primarily the result of the early part of the impact. Ripples are developing in increasing numbers around the central peak. The ring pattern in both papers is nonsymmetrical. The wave pattern has different velocities in different directions, indicating anisotropy. In the first paper sample, the main directions are inclined relative to the frame; in the second sample, they are nearly parallel to the frame. At this point, the ring pattern has not yet been influenced by reflections from the the sample frame. Therefore, the shape of the pattern is due only to the nonuniformity of the specimen.

Minor local variations in the propagating wave pattern can also be seen in the interferograms, as a disturbance in the elliptical pattern. These variations result mainly from local variations in the plate parameter, which incorporates local parameters of the paper such as density, thickness, modulus of elasticity, and the Poisson ratio. All of these factors change the wave impedance of the paper. Some of the local variations seem to be repetitive, indicating that there is some kind of ordered structure in the paper. A series of new experiments on papers with known local variations or defects should reveal some of the causes of these local variations.

Fallstrom *et al.* (*4*) proposed the use of the β parameter for anisotropic plates (Eq. 3) to derive an expression for the quotient between the effective plate stiffness in the maximum and minimum directions. They showed it to be proportional to the quotient between the two radii of anisotropy raised to the power of four. The impact is, however, modeled as a Dirac pulse (a function with infinitesimal duration in time where the time-integral equals a constant) in space and time (Case A above, which is not the case in our present experiments).

$$D_{max}/D_{min} = (r_{max}/r_{min})^4 \quad (6)$$

D is the plate stiffness defined as:

$$D = E\,h^3/\,[12(1-\nu^2)\,] \quad (7)$$

r_{max} = radius of maximum anisotropy of the ring

r_{min} = radius of minimum anisotropy of the same ring

E = effective Young's modulus in a specific direction

h = thickness of the plate

ν = the Poisson ratio.

The radius of anisotropy for each of the two samples of Fig. 5 was measured from the impact point to the outermost possible ring at 380 μs. The directional angles (θ) are also measured for both samples with the Plexiglas frame as a reference line. Results are given in **Table I**. The ratios between the maximum and minimum radii raised to the power of 4 are presented, since this measure (for a Dirac pulse impact) is equal to the ratios between the Young's moduli, assuming that the Poisson ratios are small.

Ultrasonic measurements

The samples were analyzed on commercially available equipment that operates on ultrasonic principles. Basically, this equipment measures the sound velocity in the paper which is proportional to the square root of Young's modulus (*6*). The measurement is made in the ultrasonic range. Measurements of the sound velocity over a distance of 150 mm are repeated for a number of directions covering the MD-CD plane of the paper. The angle of rotation between each measurement is 10°. The velocity ratio v_{max}/v_{min} is computed, and the angle between the maximum sound velocity and the machine direction is found (**Fig. 6**).

In Table I, the calculated ratio of the Young's modulus using the ultrasonic test method is presented for both samples. The velocity ratio v_{max}/v_{min} is squared to get the ratio for the Young's modulus. Directions of anisotropy ϕ are also given in the table.

The ultrasonic values $(v_{max}/v_{min})^2$ presented in Table I are about 25% higher than the values of $(r_{max}/r_{min})^4$. The directions of anisotropy derived ultrasonically (ϕ) compare quite well with the directions obtained from the interferograms (θ).

Discussion

Interferograms of propagating bending waves in paper show different propagation speeds in different directions. The main directions may be inclined with respect to the machine direction of the paper. The pattern shows the anisotropy of the paper. The pictures also show deviations in the wave pattern that are probably caused by local variations in the paper, either in material, geometry, or both. This finding suggests that the method may be used to study local variations. Products of paper like corrugated board or paperboard may also be studied using the same method.

Measurements of the wave speeds in the interferograms give a measure of the quotient between plate (or sample) parameters, indicating the effective sample stiffness in the two main directions of the paper. Howev-

6. The angle between the maximum sound velocity and the machine direction for each of the two samples in Fig. 5

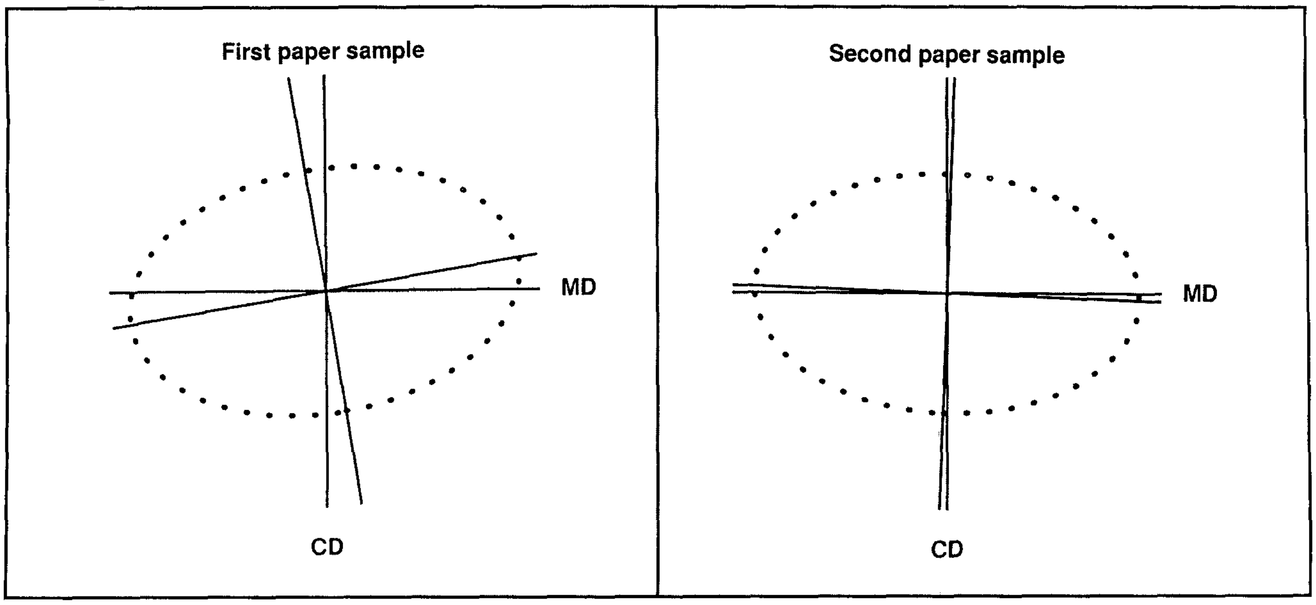

er, these values cannot be compared directly to the ultrasonically measured values for wave speeds for two main reasons. First, the assumption is invalid that the holographic measurements are made far away from the impact center both in space and time. In fact, the impact is still going on at the time represented by the comparative values in Table I, which is far from being a Dirac pulse.

Second, the Poisson ratios of the paper in both main directions are unknown but are needed in evaluating both the interferograms and the ultrasonic measurements, if the quotients of Young's modulus are to be compared.

Castagnede *et al.* (7) also reported that there is a significant difference between results of mechanical and acoustical measurements of paper. Interestingly, he reported deviations similar to those in Table I.

An analytical solution to the impacted anisotropic plate problem similar to the solutions of Cases A and B does not exist, as far as we know. However, numerical solutions to the same problem can be obtained to give improved estimates of the material parameters. These solutions can be compared to our experimental results. This approach could be rewarding since there are programs available commercially that allow computers to make such calculations.

The findings of this preliminary report demonstrate that the proposed method can be used to examine anisotropy as well as local variations in paper.□

Literature cited

1. Vest, C. M., Holographic Interferometry, Wiley, New York, 1979.
2. Aprahamian, R., Evenson, D. A., Mixson, J. S., Jacoby, J. L., Experimental Mechanics 11(8): 357(1971).
3. Fallstrom, K.-E., Gustavsson, H., Molin, N.-E., and Wahlin, A., Experimental Mechanics 29(4): 378(1989).
4. Fallstrom, K.-E., Lindgren, L.-E., Molin, N.-E., and Wahlin, A., Experimental Mechanics 29(4): 409(1989).
5. Molin, N.-E. and Jansson, E. V., J. Acoust. Soc. Am. 85(5): 2179(1989).
6. Sonic Sheet Tester Model SST-25, Operation Manual, Nomura Shoji Co Ltd.
7. Castagnede, B., Mark, R. E., and Seo, Y. B., J. Pulp Paper Sci. 15(6): 201(1989).

We are grateful to Anders Wahlin at the Division of Experimental Mechanics, Lulea University of Technology, who helped us with the measurements. This preliminary study was partly supported by the Engineering Research Council of the Swedish Board for Technical Development.

Received for review March 13, 1990.

Accepted Sept. 15, 1990.